Analyst

PAPER

View Article Online
View Journal

Cite this: DOI: 10.1039/d5an00461f

Anti-tumour and associated metabolic effects of repurposed afuresertib and taxifolin for glioblastoma treatment

Rui Chen,[a] Nurcan Gumus,†[b,c] Supisara Jearranaiprepame,[b,c,d] Alison Whitby,[c] Ruman Rahman[c] and Dong-Hyun Kim*[a,e]

Received 25th April 2025,
Accepted 1st December 2025

DOI: 10.1039/d5an00461f

rsc.li/analyst

Isocitrate dehydrogenase wild-type glioblastoma (GBM) is a particularly devastating central nervous system tumour with limited treatments. Taking advantage of computational strategies, drug repurposing has been regarded as an alternative and effective tool in GBM drug development, especially models targeting altered metabolic pathways and genomic alterations. In previous work, afuresertib and taxifolin were selected as repurposed candidates after the application of Transcriptomics-informed Stoichiometric Modelling and Network analysis. Although these two candidates have been studied in other types of cancers, they have not been tested against GBM. This study explored the *in vitro* anti-tumour effect of afuresertib and taxifolin using the PrestoBlue metabolic viability assay and Transwell collagen barrier assay on patient-derived glioblastoma cell lines. Their associated metabolic impact was revealed by the application of an untargeted metabolomics method. The results showed that afuresertib exhibited stronger inhibition of GBM cell proliferation and invasion than taxifolin. Glycerophospholipid metabolism was more active in cells derived from the invasion margin than in cells from the tumour core, indicating the possibility of varying underlining genetic mutations between GIN and GCE cell lines. Afuresertib could affect amino acid metabolism and glycerophospholipid metabolism, exerting the function of anti-proliferation and anti-invasion. Taxifolin could damage nicotinate and nicotinamide metabolism, leading to the death of tumour cells.

Introduction

Isocitrate dehydrogenase (IDH) wild-type glioblastoma (GBM) remains a particularly devastating central nervous system tumour with limited treatments.[1] Substantial inter- and intra-tumour heterogeneity and a highly invasive nature are regarded as two crucial reasons for minimal progress in effective therapies for GBM.[2] Besides, radio-/chemo-resistance and associated tumour recurrence remain confounding factors for therapy options.[3,4] There is therefore an urgent need for the discovery of effective therapies which may be rapidly repurposed for drug development for GBM.

Following the identification of IDH wild-type and mutant GBM, increasing evidence has strongly supported the notion that GBM is a metabolic disorder, generating metabolic reprogramming associated with metabolic heterogeneity.[5] Both GBM progression and invasion involve complex interactions with the metabolic environment;[6,7] however, this is not a well-understood area. To investigate the alteration of metabolism in GBM, metabolomics is a promising approach with the ability to capture metabolic signatures of a tumour's phenotype.[8] Combined with other omics approaches, several *in vitro* metabolomic studies have been conducted based on both established and primary GBM cell lines, elucidating information regarding altered metabolic pathways and potential biomarkers.[9–11] For instance, 2-hydroxyglutarate, glycerophosphocholine, and myo-inositol were reported as highly abundant in IDH mutant GBM.[12–14] These metabolic vulnerabilities of GBM can potentially provide new therapeutic opportunities.[15]

To translate these metabolic alterations into therapeutic advances, drug repurposing is an increasingly attractive proposition since it employs de-risked compounds (often with established patient safety and toxicological profiles determined for certain indications), providing multiple advantages over discovering and developing an entirely new drug.[16,17] Moreover, based on the analysis of large-scale data, compu-

[a]*Centre for Analytical Bioscience, Advanced Materials and Healthcare Technologies Division, School of Pharmacy, University of Nottingham, Nottingham, NG7 2RD, UK. E-mail: dong-hyun.kim@nottingham.ac.uk*
[b]*Molecular Therapeutics and Formulation Division, School of Pharmacy, University of Nottingham, Nottingham, NG7 2RD, UK*
[c]*Children's Brain Tumour Research Centre, Biodiscovery Institute, School of Medicine, University of Nottingham, Nottingham, NG7 2RD, UK*
[d]*National Nanotechnology Center (NANOTEC), National Science and Technology Development Agency (NSTDA), Pathumthani, 12120, Thailand*
[e]*College of Pharmacy, Kyungpook National University, Daegu 41566, Republic of Korea*
†Current address: Department of Medical Biology/Department of Medical Pharmacology, Faculty of Medicine, Izmir Bakircay University, Izmir, Türkiye.

tational approaches have primarily been employed in drug repurposing to gain meaningful interpretations for hypothesis generation, particularly through molecular pathway mapping.[18] By establishing specific disease networks based on the pathology, data from genome-wide association studies and protein/metabolite interactions, network analysis allows identification of highly connected reactions which would potentially disrupt the process of pathophysiology once inhibited.[19] In our previous study, a recombinant innovation approach was developed, termed 'Transcriptomics-Informed Stoichiometric Modelling and Network analysis' (TISMAN). By constructing GBM metabolic models using published transcriptomics datasets, TISMAN identified metabolic reactions of interest prior to screening a chemical–gene interaction database. As a result, five candidates were prioritised: afuresertib, taxifolin, pyrogallol, isorhamnetin, and formononetin.[20]

For evaluating a drug candidate's potential value for GBM therapy, it is reasoned to target the major active pathway in the disease model. The phosphatidylinositol 3-kinase-serine-threonine kinase-mechanistic target of rapamycin (PI3K-AKT-mTOR) pathway has been studied as one of the most frequently altered biochemical signalling cascades in GBM and is related to metabolic regulation of proliferation and migration, thus representing a potential target for drug development and repurposing.[21–23] Among the five selected compounds, combined with literature review, afuresertib (Fig. 1A) and taxifolin (Fig. 1B) have been reported to target the PI3K-AKT-mTOR pathway. Afuresertib, a novel AKT inhibitor, has been demonstrated to reduce the activity of AKT protein within this pathway and has shown potent anti-tumour effects, both preclinically and clinically, across various cancer types including multiple myeloma, leukaemia, oesophageal cancer and ovarian cancer, either as a monotherapy or in combination with other drugs.[24–28] However, its effects have yet to be evaluated on GBM. Taxifolin is a flavonoid, mainly exhibiting antioxidant and anti-inflammatory roles.[29–31] Yao *et al.* discovered that taxifolin could dually target PI3K and mTOR to inhibit GBM cell growth.[32] However, it should be noted that the cell lines involved were commercial ones rather than primary patient derived, and the ability to assess anti-invasion was not taken into consideration. Hence, we hypothesised that afuresertib and taxifolin could alter metabolic pathways in GBM to exert an anti-tumour phenotype.

In this study, the anti-tumour effects of repurposed afuresertib and taxifolin have been studied on patient-derived GBM cell lines and the drugs' mode of action has been inferred from a metabolomic perspective using liquid chromatography-mass spectrometry (LC-MS)-based metabolite profiling.

Materials and methods

Materials

Afuresertib (Catalog No: S7521, Batch No: 01, Purity: 99.26%) was purchased from Selleck Chemicals LLC (Berlin, Germany). Taxifolin (Catalog No: HY-N0136, Batch No: 23044, Purity:

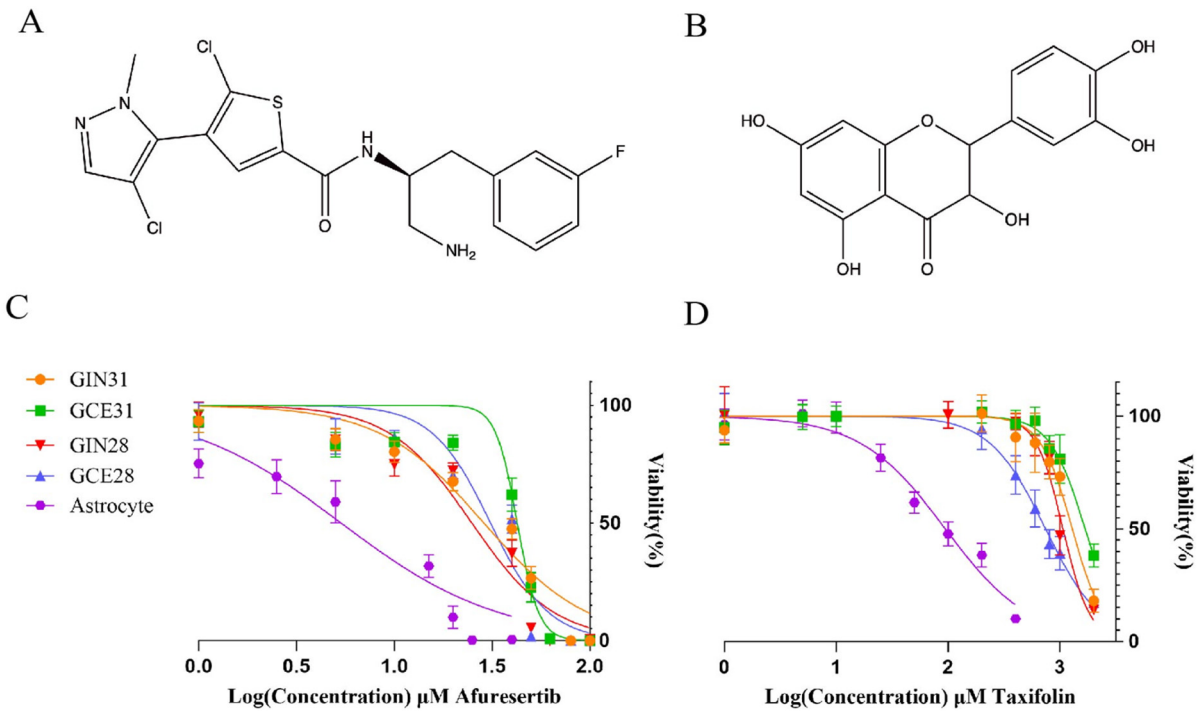

Fig. 1 The chemical structures of the repurposed drug candidates and assessment of GBM metabolic viability. (A and B) The chemical structures of afuresertib and taxifolin. (C and D) The dose-dependent inhibition of GBM cells and astrocytes exposed to treatments. The concentration of the drug is log 10 transformed. The colours and shapes represent distinct cell lines.

99.97%) was ordered from MedChemExpress LLC (Monmouth Junction, USA). PrestoBlue™ cell viability reagent (Lot: 2342788), Dulbecco's modified Eagle's medium (DMEM, Catalog No.: 31885023, Lot No.: 2436216) and 0.5% Trypsin-EDTA (10×) were purchased from Thermo Fisher Scientific Inc. (Leicestershire, UK). Dulbecco's phosphate buffered saline (DPBS), dimethyl sulfoxide (DMSO) and 0.5% Trypsin-EDTA 10× were ordered from Sigma-Aldrich Co. LLC (Gillingham, UK). Bovine growth serum supplemented calf (FBS) was purchased from Cytiva (Utah, USA). Phosphate buffered saline (PBS) solution was provided by the laboratory. The astrocyte medium kit (Lot: 34355) and 1 mg mL^{-1} poly-L-lysine (PLL, Lot: 33107) were purchased from Caltag Medsystems Ltd (Buckingham, UK). Cultrex Mouse Collagen IV (Lot: 1578996) was purchased from Bio-Techne Corporation (Minneapolis, USA). 24-Well ThinCert™ 8 μm cell culture inserts were ordered from Greiner Bio-One International GmbH (Stonehouse, UK).

Cell culture Petri dishes (100 × 20 mm) were ordered from Corning Incorporated (Flintshire, UK). Ammonium carbonate was purchased from Honeywell International Inc. (Berks, UK). LC-MS grade methanol and acetonitrile were supplied by VWR Chemicals, LLC (Lutterworth, UK). Deionised water was automatically generated from a PURA-Q+ ultrapure water purification system (Scientific Laboratory Supplies, UK).

Cell lines and culture conditions

Glioblastoma invasive margin (GIN28, GIN31) and glioblastoma contrast-enhanced core (GCE28, GCE31) cell lines were previously derived at Queen's Medical Centre from patients undergoing resected tumour surgery. These cell lines were derived from intra-tumour regions of two tumours (patient 28 and patient 31). All cell lines were cultured in antibiotic-free DMEM supplemented with 10% FBS and incubated under humidified growth conditions at 37 °C and 5% CO_2.

Cortical astrocytes (healthy counterpart of GBM cells) were purchased from ScienCell Research Laboratories, and the culture process was conducted according to the supplier's instructions.

Metabolic viability assay

5000 cells per well were seeded in 96-well plates for all patient-derived GBM cell lines. After stabilising for 24 h, the culture medium was replaced with 100 μL of drug-containing medium and incubated for a further 72 h. Multi-point doses of drug treatment were applied, ranging from 1–200 μM for afuresertib and 1–2000 μM for taxifolin, respectively. An appropriate vehicle (0.1% DMSO) and positive cell death controls (10% DMSO) were included. Fluorescence at 544/590 nm was measured using a microplate reader (FLUOstar® Omega, BMG Labtech) after 1 h of PrestoBlue™ (1 : 10) incubation. Viability of drug-treated cells was determined by normalising fluorescence intensity against that of the vehicle-only control.

For astrocytes, PLL working solution was prepared by adding 150 μL of 1 mg mL^{-1} PLL in 10 mL of sterile water. The plates were coated with 43 μL of PLL working solution overnight and rinsed with 100 μL of DPBS before seeding cells. The seeding density of astrocytes was 1600 cells per well, and multi-point doses were adopted with 1–50 μM for afuresertib and 1–500 μM for taxifolin. Two control groups were also included as above. The measurement process and data analysis were performed as previously described for GBM cell lines.

Invasion assay

To study the capability of drugs to inhibit GBM cell invasion, the Transwell collagen barrier assay was adopted to investigate the response of single cells to the drug treatment.[33] Mouse collagen IV (15 μg per insert) was added to ThinCert™ 8 μm cell culture inserts and the coated inserts were then dried in a sterile environment. Prior to seeding cells, 100 μL of DMEM was added to dried collagen and soaked for 1 h.

Digested cells were later suspended in DMEM. 100 μL of drug-containing DMEM was added to the pre-soaked insert followed by the addition of 100 μL of cell suspension. The seeding densities were 12 000 cells per insert for GIN31 and GCE31, and 14 000 cells per insert for GIN28 and GCE28. The bottom chamber was filled with 700 μL of DMEM supplemented with 10% FBS. The plates were incubated for 24 h to allow invasion to commence. For the negative control, inserts contained cells suspended in DMEM supplemented with 10% FBS, while the bottom chamber was filled with DMEM.

When the incubation period was over, cells were fixed with 700 μL of ice-cold methanol for 1 h after the medium was removed. Non-invaded cells were next removed using cotton buds, and the inserts were stained with 600 μL of 0.2% crystal violet for 15 min while protected from light. Inserts were washed with water to remove residual dye and dried overnight. Finally, cells were imaged at four different fields of view under a multi-viewing microscope (Brunel, N-510).

Metabolomics study

Sample preparation. Cells were seeded in Petri dishes and cultured in DMEM supplemented with 10% FBS to harvest 1×10^6 cells at the end of experiments. After 24 h, cells were treated with afuresertib or taxifolin followed by 72 h of incubation.

To extract intracellular metabolites, cells were quickly washed with pre-warmed PBS twice after removing the medium. Then, 1.0 mL of pre-cooled (−40 °C) methanol was added to each dish followed by rapid quenching and scraping of the cells. Cell suspensions were collected and vortexed for 1 h at 4 °C. Subsequently, the supernatant was collected after centrifugation (13 000 rpm for 5 min) at 4 °C. Next, cell extracts were dried in a vacuum centrifuge evaporator and then 70 μL of LC-MS grade methanol was used for reconstitution. Finally, the reconstituted samples were centrifuged again, and the supernatant was transferred to LC-MS vials for analysis.

A pooled quality control (QC) sample was prepared by taking 10 μL aliquots from each sample and mixed in one vial (excluding blank samples) to evaluate the robustness, performance, and stability of the analytical system.

LC-MS-based metabolite profiling. The reagent-blank samples were analysed prior to the experimental samples. Experimental samples were randomised in sequence, with QC samples ($n \geq 6$) analysed intermittently throughout the duration of the analysis. Five mixed authentic standard solutions (total 266 standards) were injected under the same conditions for metabolite identification.

Separation was performed on a ZIC-pHILIC column (5 μm, 4.6 × 150 mm) manufactured by Merck Sequant (Watford, UK) with a guard column, using a Dionex Ultimate 3000 HPLC system (Thermo Fisher Scientific, Hemel Hempstead, UK). The mobile phases consisted of 20 mM ammonium carbonate (A) and acetonitrile (B), with a linear gradient (0–15 min: 20% A to 95% A, 15–17 min: 95% A to 20% A, 17–24 min: 20% A). The injection volume was 10 μL and the flow rate was 300 μL min^{-1}. The temperatures of the autosampler and the column compartment were maintained at 4 °C and 45 °C, respectively.

Detection was conducted on a Q-Exactive Plus hybrid quadrupole-Orbitrap mass spectrometer (Thermo Fisher Scientific, Hemel Hempstead, UK) fitted with a HESI source. Data acquisition was performed in rapid polarity-switching mode with spray voltages at +4.5 kV and −3.5 kV, respectively. Other instrument settings were optimised as follows: capillary temperature, 275 °C; sheath gas flow rate, 40; aux gas flow rate, 5; sweep gas flow rate, 1; S-lens RF level, 55%. The samples were acquired at a mass resolution of 70 000 at m/z 200, across an m/z range of 70–1050 with an automatic gain control (AGC) of 3×10^6. Top 10 data-dependent MS/MS (ddMS/MS) analyses were performed on QC samples at a mass resolution of 17 500 with an AGC target of 1×10^5 and stepped normalised collision energies of 20, 30 and 40.

Metabolite identification. Total ion chromatograms generated using LC-MS, including experimental samples, QC samples, and blank samples, were examined in Xcalibur (Thermo Fisher Scientific, Waltham, USA). Raw datasets were subsequently imported into Compound Discover 3.3 SP1 (Thermo Fisher Scientific, Waltham, USA) for peak picking, peak alignment, metabolite identification and gap filling, by applying an untargeted metabolomic workflow with the retention time ranging between 0.5 and 23.5 min, peak rating results (>5), and aligned window (within m/z 5 ppm) for precursor and fragment ions. Ions were identified and annotated by matching accurate masses of detected ions with metabolites in the Human Metabolites Database (HMDB),[34] the accurate masses and retention times of authentic standards, mzCloud fragmentation database and in-house Thermo Scientific mzVault spectral libraries.

Ultimately, metabolites were classified into four levels of confidence according to the Metabolomics Standards Initiative scale.[35,36] Level 1 confidence was that the ions matched with the accurate masses, retention times, and fragments of authentic standards. Level 2 confidence represented ions matched with the exact masses and fragments of metabolites in spectral/online libraries in the absence of standards. Level 3 confidence was that ion identification was based only on accurate mass matching with database entries, without supportive fragmentation information. Level 4 confidence referred to ions only with or without predicted molecular formulas.

Pathway analysis and network mapping. In this study, metabolites with level 1 and level 2 identification confidence were applied to the pathway analysis. Pathway analysis was conducted using the online platform of MetaboAnalyst v5.0.[37] Non-human putative metabolites were excluded.

Statistics. For viability and invasion assays, curve fitting of inhibition and statistical data analysis was performed on GraphPad Prism v8.2.1 (GraphPad Software, San Diego, USA). p value <0.05 was considered statistically significant.

For univariate analysis of metabolomic datasets, the data were log-transformed. Two-tailed Student's t-test p values were adjusted using the Benjamini–Hochberg correction for false discovery rates, compensating for the multiple testing problem. An adjusted p value <0.05 was regarded as significant.

Multivariate analysis, including principal component analysis (PCA) and orthogonal partial least squares discriminant analysis (OPLS-DA), was performed on SIMCA-P v16 (Umetrics, Sweden) to determine significant metabolites. After logarithmic transformation, the methods of Unit-Variance scaling (UV scaling) and Pareto scaling (Par scaling) were used for PCA and OPLS-DA, respectively.

Results

Metabolic viability

After 72 h of incubation, metabolic viability was measured using PrestoBlue™, which is a non-toxic, resazurin-based cell health indicator.[38] Metabolically active cells reduce non-fluorescent resazurin to fluorescent resorufin.[39] The intensity of fluorescence is relatively linear to the number of living/metabolically active cells. The viability results upon acute exposure to afuresertib and taxifolin are shown in Fig. 1C and D. The IC_{50} concentrations of both compounds against GBM cell lines and astrocytes are summarised in Table 1.

Results indicate that both afuresertib and taxifolin show dose-dependent impairment of metabolic viability. Afuresertib was identified as more potent in inhibiting GBM proliferation relative to taxifolin. Moreover, the cells derived from the invasion margin of GBM (GIN31/28) were more sensitive to afuresertib than their counterpart cells derived from the tumour core (GCE31/28). Astrocytes were also included to explore the selectivity of drug candidates in healthy counterpart cells. The results showed that astrocytes were more sensitive to all candidates than GBM cells, indicating that potential toxicity might exist during clinical practice.

Table 1 The IC_{50} values of afuresertib and taxifolin for GBM cells and astrocytes (μM)

Name	Astrocytes	GIN31	GCE31	GIN28	GCE28
Afuresertib	5.353	28.75	42.54	24.95	31.09
Taxifolin	90.20	1287	1676	1067	742.8

LC-MS-based metabolite profiling. After investigating the anti-tumour effects of candidates, LC-MS-based metabolite profiling was employed to explore which metabolites and metabolic pathways were affected or altered by the drug exposure. In order to improve the quality of input data, features were regarded as non-informative and removed if their relative standard deviations (RSD) were ≥30% in the technical replicates of pooled QC samples.[40]

For high dimensional datasets, PCA and OPLS-DA are commonly used to construct models that classify samples and distinguish metabolite variations across different experimental conditions. In this study, the information on mass ion pairs (retention time, *m*/*z*, abundance) was imported to SIMCA-P for model construction.

PCA models were first built to evaluate the similarities among the variables and the robustness of the analytical system. In the PCA score plots (Fig. S1), the pooled QC samples were clustered tightly towards the centre, indicating that satisfactory stability of the instrument was achieved. Within each group, none of the samples were analysed as an outlier and no significant differences were observed, further evidencing that the experimental setup was carefully conducted. Clear clustering and separation for different drug treatment and control groups were observed, indicating that these were associated with metabolic alterations resulting from drug exposure.

Next, OPLS-DA models were constructed to identify metabolites with significant changes in abundance between the drug-treated and control groups. In the OPLS-DA score plots, drug-treated and control groups were clearly clustered and separated, indicating significant distinction of the metabolic profiles. However, OPLS-DA is a supervised method with a risk of overfitting the dataset. To evaluate the fitness of model, cross validation and permutation methods (999 times) were further verified. The cross-validation results of OPLS-DA models are summarised in Table S1. An R^2Y and Q^2 value of 0.50 is recommended for cross validation where the model is regarded as accurate.[41] The results of cross validation in this study were excellent as the values of R^2Y and Q^2 in each model were ≥0.90. Permutation testing for each OPLS-DA model met the SIMCA-P validity criteria: the original R^2Y and Q^2 values were higher than those of all permuted models, the Q^2 regression line had a negative intercept, and the R^2Y and Q^2 regression lines decreased from the original to the permuted models, confirming that the models were not overfitted. Combined with cross validation and permutation results, the models constructed in this study were less likely to overfit our dataset, with good fitness and good predictive ability. Lastly, lists of variable importance in projection (VIP) scores based on the OPLS-DA models were generated for each comparison. VIP values generally represent the importance of each variable in the OPLS-DA model and have been used to extract the metabolites related to separation. In addition, the adjusted *p* value of <0.05 generated from the univariate analysis was combined to select significantly altered metabolites. Hence, in this study, the metabolites with VIP >1 and adjusted *p* value <0.05 were considered as significantly altered compounds.

Metabolic variation across untreated GBM cells from distinct intra-tumour regions. As determined by the PCA score plots, the cells derived from invasive margin (GINs) and the cells derived from the tumor core (GCEs) have been clearly separated. Plots indicated that there were some metabolic differences between respective GINs and GCEs, despite being derived from the same patient tumour.

Volcano plots were next used to visually select significantly altered metabolites by combining the statistical *p* value and fold change (FC) between two groups. The volcano plots of GIN31/GCE31 and GIN28/GCE28 are shown in Fig. S2, where metabolites with FC >2 and adjusted *p* value <0.05 are highlighted. The number of identified metabolites abundant in GIN31 is greater than that identified in GCE31. However, the number of identified metabolites abundant in GIN28 is less than that identified in GCE28. The results of univariate analysis therefore suggest that intra-tumour metabolic heterogeneity is evident within each patient-derived cell line.

Using well-constructed OPLS-DA models (Fig. 2A and B), cells from the invasive margin and tumour core were clearly separated, and the significantly altered compounds contributing to this separation are shown in Tables S2 and S3.

All the identified metabolites were next submitted to MetaboAnalyst v5.0 for pathway analysis. Pathway analysis performs a vital function in interpreting high dimensional molecular datasets.[42] In MetaboAnalyst v5.0, pathway analysis consists of network analysis and pathway topology analysis. Such networks are a powerful tool for the representation of metabolic pathways. Pathway topology analysis not only lists the components of pathways but also describes their interaction.[43] Based on the existing knowledge of biological pathways, metabolites are expected to be mapped onto pathway sets, representing how these metabolites collectively function and interact in biological (healthy and diseased) contexts.

The analysis revealed biochemical signaling and biological processes that are most significantly altered between each untreated cell line, enriching our understanding of the intrinsic metabolomic profiles of GBM cells propagated *in vitro*. The results of the pathway analysis for GIN31/GCE31 are shown in Fig. 2C. A total of 58 metabolic pathways were initially identified, which were then filtered to 23 significant metabolic pathways with adjusted *p* value <0.05 and impact factor >0.1 (shown in Table S4). Among these 23 metabolic pathways, most metabolites were related to amino acid metabolism, and those related to glycerophospholipid/sphingolipid metabolism were more abundant in GIN31. Only metabolites mapped to taurine and hypotaurine metabolism were more abundant in GCE31. Hence, compared to GCE31, GIN31 cells had more active metabolic pathways which were associated with higher demand in energy production, amino acid biosynthesis and phospholipid biosynthesis.

The pathway analysis results for untreated GIN28/GCE28 are shown in Table S5. In contrast to GIN31/GCE31, GCE28 cells are more metabolically active than GIN28 cells, with metabolites mapping to pathways including lysine degradation, alanine, aspartate and glutamate metabolism, nicoti-

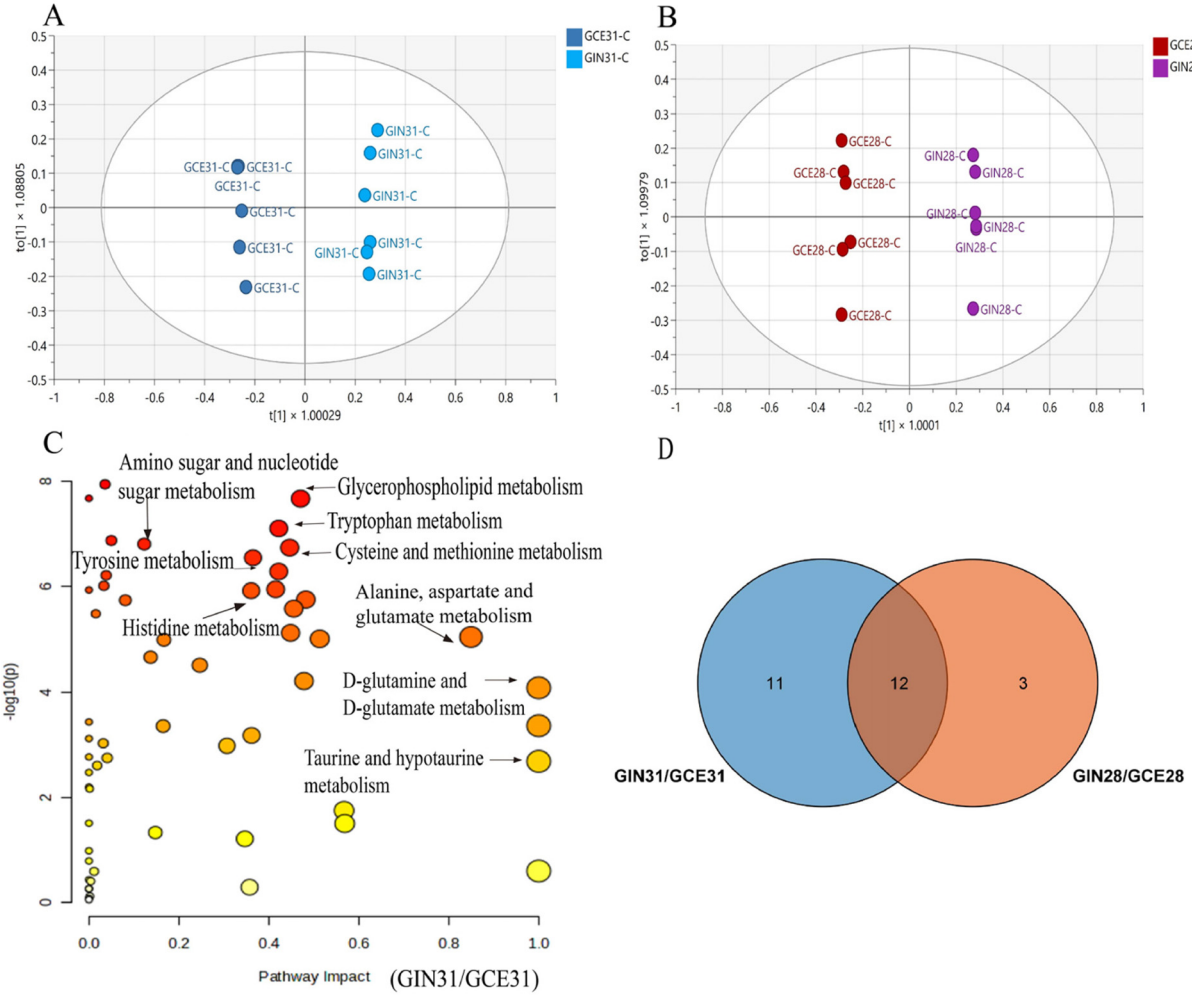

Fig. 2 Metabolic variation between GBM cells derived from the invasive margin and tumour core. (A and B) The score plots of the constructed OPLS-DA models for GINs/GCEs. The cross-validation results were R^2Y = 0.997 and Q^2 = 0.951 for GIN31/GCE31, and R^2Y = 0.999 and Q^2 = 0.927 for GIN28/GCE28. (C) The result of pathway analysis for GIN31/GCE31. The colour (white to red) represents statistical significance. The size of the bubble is directly related to the number of metabolites mapped on the specific pathway. The pathway impact factor represents the importance of the identified pathway in the whole metabolic network. (D) Venn diagram of the number of identified metabolic pathways when comparing metabolic differences between GINs and GCEs.

nate and nicotinamide metabolism, arginine and proline metabolism, and glycine, serine and threonine metabolism. Collectively, the results of pathway analysis were consistent with the results of univariate analysis presented previously in the volcano plots, indicating the heterogeneity existing between and within patient-derived GBM cell lines.

Despite the observed differences existing between cell lines derived from two patients, shown in Fig. 2D, 12 shared significant pathways were identified in both GIN31/GCE31 and GIN28/GCE28, including alanine, aspartate and glutamate metabolism, glycerolipid metabolism, glycerophospholipid metabolism, glyoxylate and dicarboxylate metabolism, serine and threonine metabolism, lysine degradation, amino sugar and nucleotide sugar metabolism, sphingolipid metabolism, cysteine and methionine metabolism, glycine, serine and threonine metabolism, arginine and proline metabolism, and pentose and glucuronate interconversions. Even though the major metabolic patterns of GINs and GCEs were distinct, metabolites which mapped to glycerophospholipid metabolism showed a similar trend. These metabolites included phosphatidyl choline (PC), phosphatidyl ethanolamine (PE), and phosphatidyl serine (PS), which all exhibited higher abundance in GINs, except for choline phosphate, shown in Fig. 3. Additionally, other metabolites which were mapped onto glycerolipid metabolism and sphingolipid metabolism were more abundant in GIN cells, including serine, sphinganine, and *sn*-glycerol 3-phosphate.

Changes in glycerophospholipids and their metabolites are closely related to cell membrane fluidity, adhesion, apoptosis, proliferation, invasion, metastasis, angiogenesis, and lymphoangiogenesis.[44,45] In cancer cells, increased PC synthesis affects cellular proliferation and programmed cell

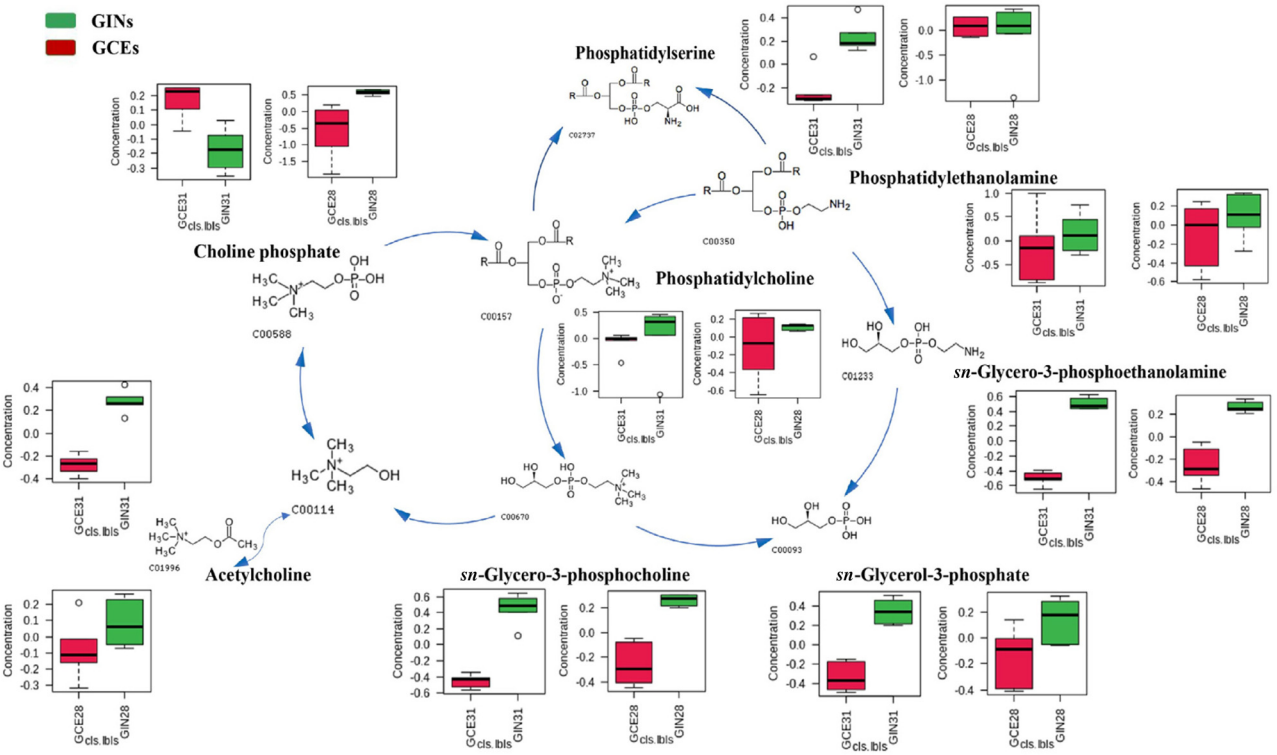

Fig. 3 The glycerophospholipid metabolism pathway and the abundance of metabolites identified in GINs and GCEs. The normalised abundances of PC, PE, PS and their metabolites are shown for GCE cells in red and GIN cells in green. The abundance of metabolites was exported from MetaboAnalyst 5.0 and reflects scaled data for visualisation.

death.[46] Moreover, the larger amounts of PS and PE exposed on the surface of GBM cell membranes compared with healthy cells increase the negative charges on the outer surface of membranes, inducing mutual repulsion and promoting tumour cell migration.[45,47] Collectively, the high abundance of PC, PE, PS and their metabolites could be associated with GINs being derived from the infiltrative margin of the tumour tissue, indicating their potential as putative metabolic biomarkers for discriminating GINs and GCEs.

Furthermore, phosphatidylinositols are another class of glycerophospholipids which are important mediators of several signalling pathways.[48] It has been reported that the 1-phosphatidyl-1D-myo-inositol-4-phosphate metabolic pathway is related to cell metastasis.[49] Its downstream metabolite, myo-inositol, was identified at higher abundance in GIN28 compared with that in GCE28, although not detectable in either GIN31 or GCE31, further indicating that this pathway may contribute to the differential metastatic potential observed between GINs and GCEs.

The metabolic pathways altered in GIN/GCE cells upon afuresertib treatment. To investigate the metabolic pathways affected by drug treatment, the results of pathway analysis and selected significant pathways for each cell line after afuresertib treatment are summarised in Tables S6–S9.

As shown in Fig. 4A, compared with the untreated group, 14 significant pathways were identified in GIN31 after afuresertib treatment, and 6 metabolic pathways were identified for GCE31. The pathways identified in GIN31 and GCE31 showed high similarity as 5 pathways were shared in both cell lines. A similar phenomenon was observed in GIN28 and GCE28, indicating that afuresertib might exert a similar downstream effect in cells derived from different tumour locations from the same patient. Four metabolic pathways were identified which were shared by all four GBM cell lines upon afuresertib exposure, including alanine, aspartate and glutamate metabolism, histidine metabolism, cysteine and methionine metabolism, and glycerophospholipid metabolism.

Afuresertib treatment broadly suppressed amino acid metabolism in GBM cells. The level of alanine, which replenishes the nutrient sink for rapidly proliferating GBM cells,[50] was decreased. The glutamate and glutamine cycle, typically upregulated to meet the requirement for biosynthesis of proteins, lipids, and nucleic acids,[51] was also disrupted. Their abundance was decreased, along with aspartate, a downstream product of glutamine oxidation, crucial for protein and nucleotide biosynthesis.[52] Exogenous methionine, essential for GBM colony formation and survival *in vitro*,[53] showed reduced abundance. The levels of other amino acids, including phenylalanine and tryptophan, were decreased in some GBM cells that received treatment, although they were not identified as major altered pathways. Collectively, these reductions indicate that afuresertib exerts its anti-tumour activity by limiting

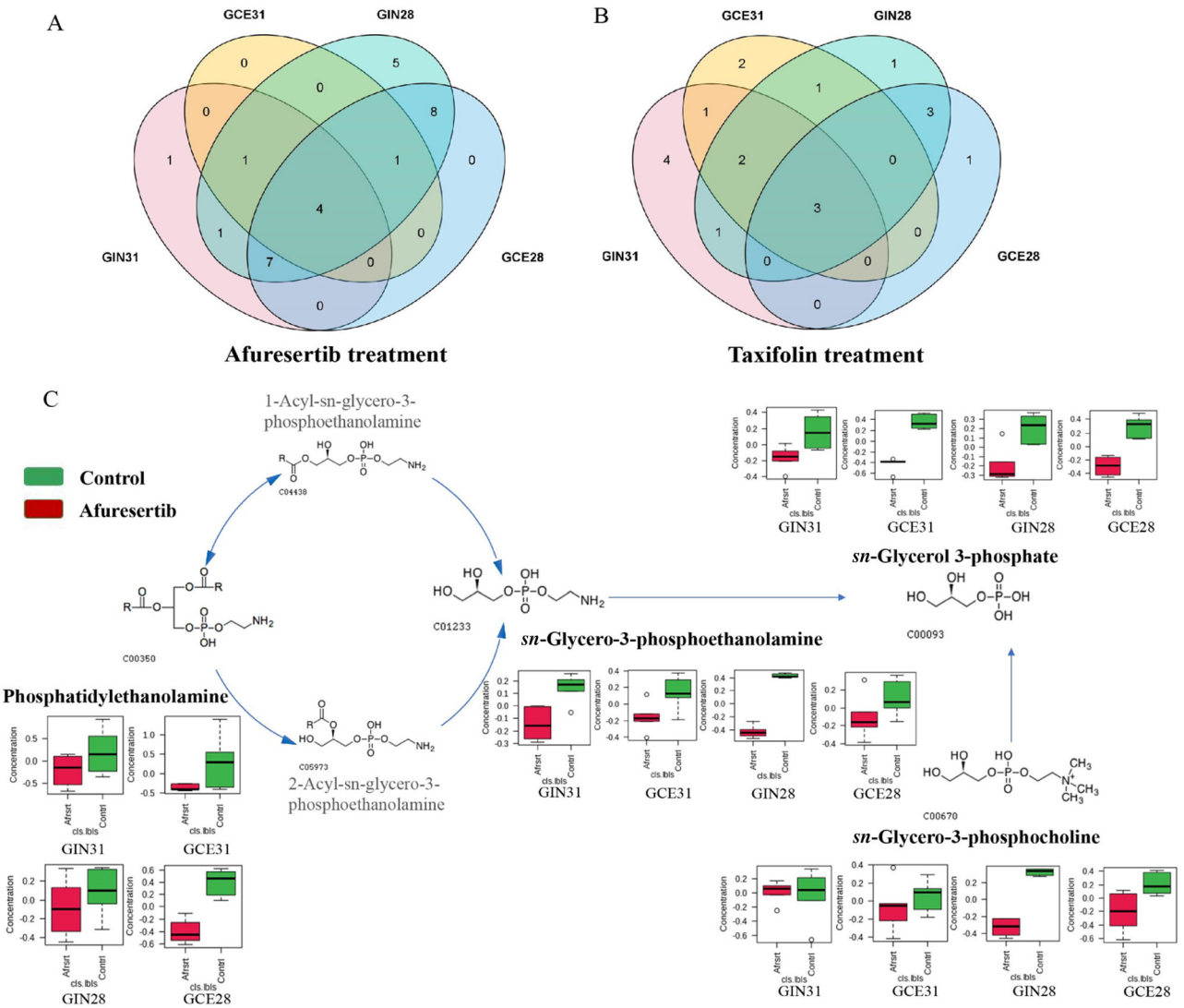

Fig. 4 Metabolic alteration of GBM cells upon acute afuresertib treatment. (A) Venn diagram depicts the number of altered metabolic pathways in GBM cell lines after afuresertib treatment. (B) Venn diagram depicts the number of altered metabolic pathways in GBM cell lines after taxifolin treatment. (C) The normalised abundance of altered metabolites mapped to the glycerophospholipid metabolism pathway in GBM cell lines upon afuresertib treatment, shown for GCE cells in red and GIN cells in green. The abundance of metabolites was exported from MetaboAnalyst 5.0 and reflects scaled data for visualisation.

the availability of amino acids necessary for tumour survival and progression.

In addition, the abundance of metabolites involved in glycerophospholipid metabolism was lower in afuresertib-treated cells (Fig. 4C). Given that alterations in glycerophospholipid metabolism can affect cell membrane composition, fluidity, and downstream signalling, afuresertib may also induce cell death by disrupting membrane integrity and impairing signalling pathways.

The metabolic pathways altered in GIN/GCE cells upon Taxifolin treatment. The identified significant pathways for each cell line upon taxifolin treatment are summarised in Tables S6–S9. As shown in Fig. 4B, only 3 pathways were shared for all tested GBM cell lines after taxifolin exposure (histidine metabolism, nicotinate and nicotinamide metabolism and glycerophospholipid metabolism).

Compared to untreated cells, taxifolin treatment resulted in reduced levels of several metabolites involved in histidine metabolism, including histidine, histamine, aspartate, and glutamate. Apart from that, the abundance of metabolites associated with nicotinate and nicotinamide metabolism was also decreased (Fig. 5B). Nicotinamide adenine dinucleotide (NAD^+) and its degradation products are key regulators of glycolysis, oxidative phosphorylation and the tricarboxylic acid (TCA) cycle.[54] Our results indicated that taxifolin may interfere with cellular energy metabolism by lowering these critical metabolites. Moreover, NAD^+ acts as a substrate for multiple downstream signalling pathways, including DNA repair, post-

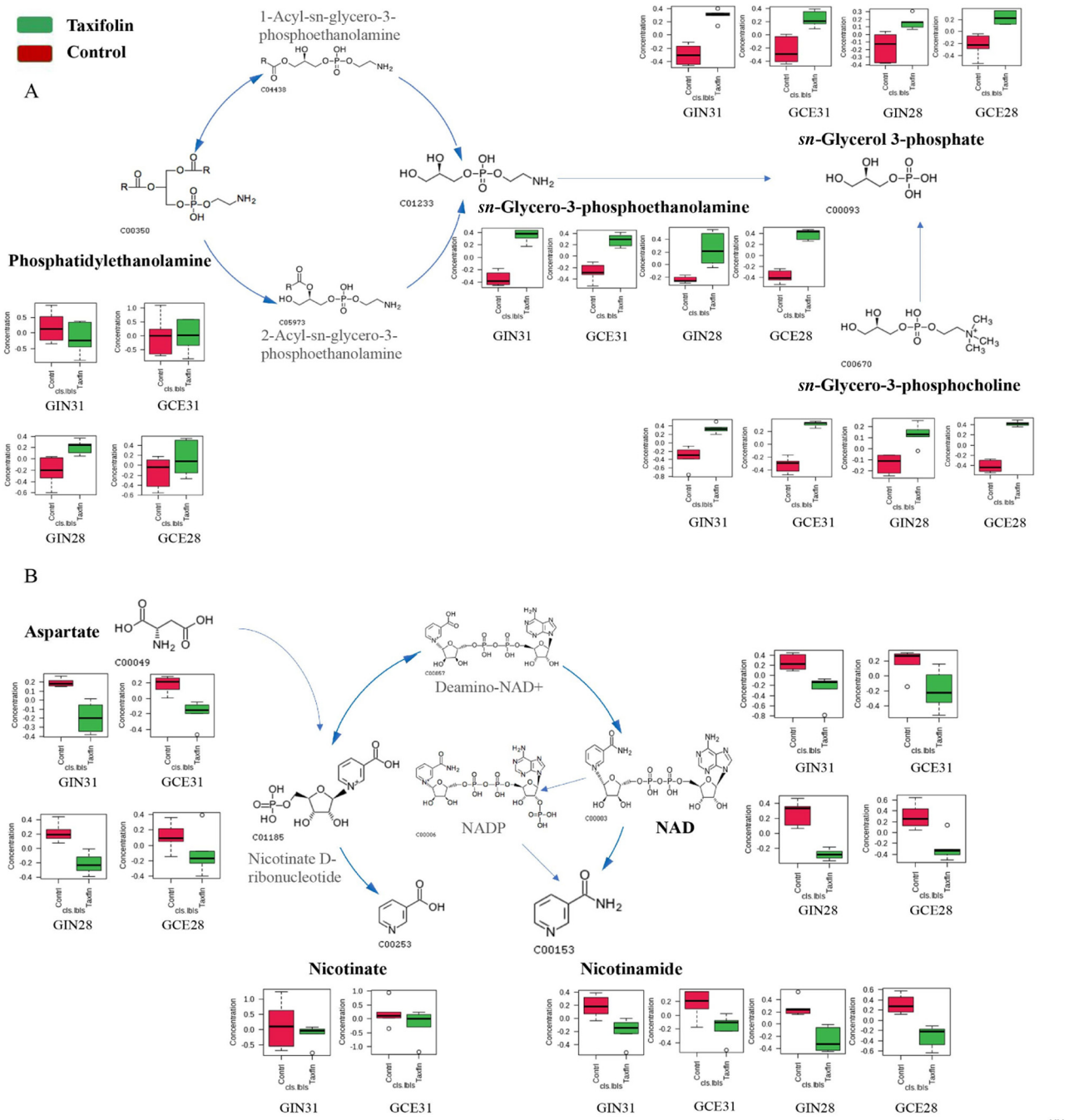

Fig. 5 Metabolic pathways altered by taxifolin treatment. (A) The abundance of metabolites related to glycerophospholipid metabolism after taxifolin treatment. (B) The abundance of metabolites mapped to nicotinate and nicotinamide metabolism after taxifolin treatment. The normalised abundances of identified metabolites are shown for untreated cells in red and taxifolin-treated cells in green. The abundance of metabolites was exported from MetaboAnalyst 5.0 and reflects scaled data for visualisation.

translational modification, inflammatory response, and apoptosis.[55] The observed reduction suggested that taxifolin may further disrupt these processes, associated with impaired metabolic activity.

Glycerophospholipid metabolism was also identified as a significant pathway in GBM cells exposed to taxifolin. In contrast to afuresertib treatment, the abundance of metabolites in this pathway were identified at a higher level in treated cells (Fig. 5A). The results indicated that taxifolin may not inhibit glycerophospholipid metabolism.

Distinct metabolic patterns between untreated GBM cells and astrocytes. To understand whether these identified metabolic pathways affected by afuresertib and taxifolin are specifically related to GBM disease, experiments were repeated to

compare the metabolic difference between GBM cells and astrocytes. The GBM cell lines were first successfully adapted to the astrocyte medium.

The astrocytes and GBM cells were clearly separated in the score plots of both PCA and OPLS-DA (shown in Fig. S3, S4 and Table S10), indicating the distinct metabolic differences existing among groups. As shown in Fig. S5, six metabolic pathways (adjusted p value <0.05 and impact factor >0.1) were shared across the comparisons of astrocytes *vs.* GBM cells – alanine, aspartate and glutamate metabolism, sphingolipid metabolism, glutathione metabolism, glycerophospholipid metabolism, the TCA cycle, and taurine and hypotaurine metabolism.

As shown in Fig. S6, the abundance of metabolites mapped to glycerophospholipid metabolism was at higher levels in GBM cells, indicating that this pathway is more active in GBM cells relative to astrocytes. The level of hypotaurine was also higher in GBM cells relative to astrocytes, consistent with studies which reported that the hypotaurine level in tumour tissue was significantly higher than that in adjacent control tissue.[56,57] In addition, a higher level of glutathione was observed in GBM cells. It has been reported that increased glutathione has a positive association with chemo-resistance in GBM.[58–60]

The metabolic differences between GINs and GCEs were also observed when cells were cultured in the astrocyte medium. As determined from the volcano plots (Fig. S7) and pathway analysis, the data showed a similar trend to those generated from the DMEM medium, providing supportive evidence that adapting GBM cells to the astrocyte medium did not change the metabolic pattern between GBM cells.

Metabolic pathways altered in astrocytes upon drug treatment. Although no selectivity of either afuresertib or taxifolin was observed between GBM cells and astrocytes based on the metabolic viability results, drug treatment of astrocytes was still valuable to assess significant changes in metabolites and metabolic pathways, comparing these effects with those observed in GBM cells. This approach aimed to further explore whether the previously identified pathways affected by the two drugs were specifically associated with anti-tumour functions.

The control and drug treatment groups were clearly separated in PCA and OPLS-DA score plots (Fig. S8), indicating distinct metabolic differences between untreated and treated astrocytes.

As previously mentioned, after afuresertib treatment, four metabolic pathways were commonly affected across all GBM cell lines. Of these, three pathways (alanine, aspartate and glutamate metabolism, histidine metabolism, and glycerophospholipid metabolism), were also altered in astrocytes. Similarly, the three pathways affected in GBM cells following taxifolin exposure were also identified in astrocytes that received taxifolin treatment.

Metabolites (except for aspartate) involved in nicotinate and nicotinamide metabolism showed lower abundance in the taxifolin-treated group compared to controls. Additionally, metabolites mapped to glycerophospholipid metabolism displayed lower abundance in the afuresertib-treated group but higher abundance in the taxifolin-treated group, compared with controls (Fig. S9).

These findings suggest that the metabolic pathways altered by these drugs were not tumour specific as drug-induced metabolic responses in astrocytes were consistent with those observed in GBM cells. Additionally, the consistent drug response observed in both GBM cells and astrocytes supported the proposed mechanism of action from a metabolomics perspective.

Invasion assay

As discussed previously, changes in glycerophospholipids and their metabolites are closely related to cell membrane fluidity, adhesion and invasion. Based on the results of the metabolomics study, the metabolites involved in glycerophospholipid metabolism were at lower abundance upon afuresertib treatment but not upon taxifolin treatment. Hence, we next investigated the ability of afuresertib and taxifolin to inhibit cell invasion.

The results are presented in Fig. 6 and Fig. S10. Considering the comparison of the number of invaded cells between control and drug-treated groups, afuresertib significantly inhibited the ability of GBM cells to invade through the collagen barrier in a concentration-dependent manner. No statistical difference was observed between the taxifolin treated and control groups across all cell lines, indicating that taxifolin did not inhibit the GBM cell invasion within this experimental context.

Discussion

In order to develop an effective therapeutic approach for GBM, its pharmacokinetic profile, molecular mechanism, and safety need to be fully investigated. Clinically, single-agent afuresertib has shown a favourable pharmacokinetic and safety profile, with a maximum tolerated dose of 125 mg day^{-1}.[61] However, its ability to penetrate the blood–brain barrier has not been reported, raising uncertainty about its therapeutic potential in brain tumours *in vivo*. The safety of taxifolin has been well studied and toxic effects from overdose have not been reported, including mutagenicity, embryotoxicity and immunotoxicity.[62] Taxifolin was detectable in rat brain.[63] However, its low bioavailability (approximately 0.17%) presents a main limitation for clinical use.[64] Hence, given our *in vitro* findings, clear molecular mechanism, and reported clinical safety, afuresertib is a promising anti-GBM candidate.

Based on the results of the viability tests, GINs were more sensitive to afuresertib than GCEs, and the mechanism underlying this difference is unknown. Given that afuresertib is an AKT inhibitor, to explore this further, the difference in AKT gene expression was measured between GINs and GCEs. The results showed that the heterogeneity of GBM was evident at the genetic level (Fig. S11). Although the qPCR results did not directly explain the differences in sensitivity, they underscore

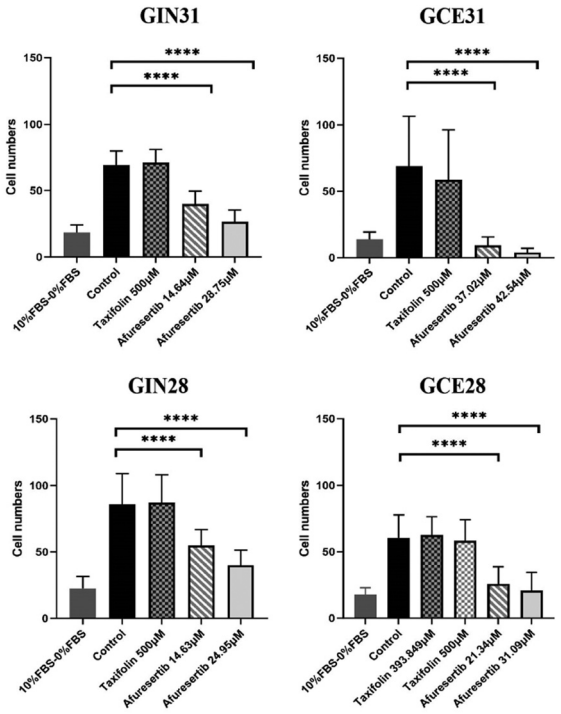

Fig. 6 Assessment of putative anti-invasion effects on GBM cells upon afuresertib and taxifolin treatment. The Transwell collagen-barrier assay was adopted to investigate the anti-invasion ability of repurposed candidates on four GBM cell lines. Two concentrations of afuresertib (IC_{25} and IC_{50}) were tested on four cell lines, while only 500 μM taxifolin was tested on GBM cells, except for GCE28. The invaded cells were fixed before being stained with 0.2% crystal violet. Images from four different fields of view were taken under a light microscope (10×) and the number of invaded cells was counted.

the complexity of gene regulation, as gene expression does not necessarily correlate with protein levels. Further investigation of AKT protein expression combined with gene expression may better elucidate these mechanisms.

Although *in vitro* metabolic viability and metabolomics results showed no selectivity of drugs between tumour and healthy cells, further investigation is still worth. Since laboratory-cultured astrocytes are required to be in a progenitor state (to permit propagation), this does not reflect the majority of astrocytes in the GBM tumour microenvironment, which are terminally differentiated (post-mitotic) mature cells, and therefore likely to be less sensitive to intracellular drug uptake.[65] This suggests that clinically there may be a therapeutic window which has not been replicated *in vitro*. Therefore, a patient-derived rodent xenograft model with predominance of post-mitotic astrocytes will be a more accurate model to determine a tolerated dose and a potential therapeutic window.

This study revealed intra-tumour metabolic heterogeneity in GBM at the cellular level. In our previous work on metabolic heterogeneity in IDH wild-type GBM primary tissue, regional heterogeneity was found in glycolysis, the TCA cycle and energy-related metabolites. For example, invasive regions were rich in D-glucose and citrate, while non-invasive areas showed higher levels of ATP and NADH.[66] These patterns were not observed in the current study, likely due to differences in patient samples and the use of cell lines rather than primary tumour tissue.

Glycerophospholipid metabolism was identified as more active in GINs than in GCEs, indicating potential variability in underlying genetic or epigenetic mutations within GINs and GCEs. From the perspective of metabolomics, our results add to the knowledge base and rationale supportive of deriving GBM cell lines from different regions. Upon drug treatment, glycerophospholipid metabolism was also identified as a significantly altered pathway in GBM cells. Combined with the results from the invasion assay, we hypothesise that afuresertib impairs invasion *in vitro* by perturbing glycerophospholipid metabolism. To test this hypothesis directly, metabolites should be extracted from drug-treated cells within the Transwell invasion chamber and subjected to metabolomic profiling.

Conclusions

This study evaluated the potential of repurposed afuresertib and taxifolin for GBM treatment *in vitro* and revealed their potential anti-tumour metabolic mechanisms. The observed anti-tumour phenotypes upon drug exposure provide evidence that these compounds are sufficient to induce these phenotypes *in vitro*, despite being agnostic about whether they are necessary *in vivo*. Further assessment of drug efficacy in GBM xenograft models will be required to validate these findings.

We cannot conclude that our *in vitro* findings fully represent GBM tumour tissue, unless metabolic changes are associated with underlying genetic or epigenetic mutations which are maintained with high fidelity in culture conditions. Our data do not determine what proportion of the observed metabolic profiles in untreated GBM cells is related to *in vitro* propagation and which is representative of *in situ* tumour metabolism. Future work will need to cross-validate these *in vitro* profiles against primary tumour infiltrative margin tissue. Nevertheless, the observed anti-tumour phenotypes upon afuresertib and taxifolin exposure provide evidence that these drug compounds are sufficient to induce these phenotypes *in vitro*, despite being agnostic about whether they are *necessary in vivo*. Further studies to assess drug efficacy in GBM orthotopic xenograft models will be required to validate these findings.

Author contributions

R. C.: investigation, methodology, data analysis, and manuscript writing; N. G.: support for cell culture, sample preparation, and manuscript reviewing; S. J.: support for qPCR analysis, sample preparation, and manuscript reviewing; A. W.: support for sample acquisition, data analysis, and manuscript reviewing; R. R. and D.-H. K.: supervision, project management, conceptualisation, and draft editing and revision.

Conflicts of interest

There are no conflicts to declare.

Data availability

The original data presented in the study will be openly available after acceptance in the Nottingham Research Data Management Repository at https://rdmc.nottingham.ac.uk/.

Supplementary information (SI) is available. See DOI: https://doi.org/10.1039/d5an00461f.

Acknowledgements

This work was supported by the University of Nottingham Centre for Analytical Bioscience (School of Pharmacy), and Children's Brain Tumour Research Centre (School of Medicine).

References

1 M. Weller, M. van den Bent, M. Preusser, E. Le Rhun, J. C. Tonn, G. Minniti, M. Bendszus, C. Balana, O. Chinot, L. Dirven, P. French, M. E. Hegi, A. S. Jakola, M. Platten, P. Roth, R. Ruda, S. Short, M. Smits, M. J. B. Taphoorn, A. von Deimling, M. Westphal, R. Soffietti, G. Reifenberger and W. Wick, *Nat. Rev. Clin Oncol.*, 2022, **19**, 357–358.

2 A. Hatoum, R. Mohammed and O. Zakieh, *Cancer Manage. Res.*, 2019, **11**, 1843–1855.

3 S. Jiapaer, T. Furuta, S. Tanaka, T. Kitabayashi and M. Nakada, *Neurol. Med. Chir.*, 2018, **58**, 405–421.

4 R. Liu, X. P. Qin, Y. Zhuang, Y. Zhang, H. B. Liao, J. C. Tang, M. X. Pan, F. F. Zeng, Y. Lei, R. X. Lei, S. Wang, A. C. Liu, J. Chen, Z. F. Zhang, D. Zhao, S. L. Wu, R. Z. Liu, Z. F. Wang and Q. Wan, *Cancer Med.*, 2018, **7**, 2848–2859.

5 C. B. Crivii, A. B. Bosca, C. S. Melincovici, A. M. Constantin, M. Marginean, E. Dronca, R. Sufletel, D. Gonciar, M. Bungardean and A. Sovrea, *Cancers*, 2022, **14**, 1092.

6 J. L. Izquierdo-Garcia, P. Viswanath, P. Eriksson, M. M. Chaumeil, R. O. Pieper, J. J. Phillips and S. M. Ronen, *PLoS One*, 2015, **10**, e0118781.

7 T. T. Lah, M. Novak and B. Breznik, *Semin. Cancer Biol.*, 2020, **60**, 262–273.

8 K. Jaroch, P. Modrakowska and B. Bojko, *Metabolites*, 2021, **11**, 315.

9 A. A. Mohan, W. H. Tomaszewski, A. P. Haskell-Mendoza, K. M. Hotchkiss, K. Singh, J. L. Reedy, P. E. Fecci, J. H. Sampson and M. Khasraw, *Front. Oncol.*, 2021, **11**, 696402.

10 C. Lu, P. S. Ward, G. S. Kapoor, D. Rohle, S. Turcan, O. Abdel-Wahab, C. R. Edwards, R. Khanin, M. E. Figueroa, A. Melnick, K. E. Wellen, D. M. O'Rourke, S. L. Berger, T. A. Chan, R. L. Levine, I. K. Mellinghoff and C. B. Thompson, *Nature*, 2012, **483**, 474–478.

11 P. Chinnaiyan, E. Kensicki, G. Bloom, A. Prabhu, B. Sarcar, S. Kahali, S. Eschrich, X. Qu, P. Forsyth and R. Gillies, *Cancer Res.*, 2012, **72**, 5878–5888.

12 L. B. Wang, A. Karpova, M. A. Gritsenko, J. E. Kyle, S. Cao, Y. Li, D. Rykunov, A. Colaprico, J. H. Rothstein, R. Hong, V. Stathias, M. Cornwell, F. Petralia, Y. Wu, B. Reva, K. Krug, P. Pugliese, E. Kawaler, L. K. Olsen, W. W. Liang, X. Song, Y. Dou, M. C. Wendl, W. Caravan, W. Liu, D. Cui Zhou, J. Ji, C. F. Tsai, V. A. Petyuk, J. Moon, W. Ma, R. K. Chu, K. K. Weitz, R. J. Moore, M. E. Monroe, R. Zhao, X. Yang, S. Yoo, A. Krek, A. Demopoulos, H. Zhu, M. A. Wyczalkowski, J. F. McMichael, B. L. Henderson, C. M. Lindgren, H. Boekweg, S. Lu, J. Baral, L. Yao, K. G. Stratton, L. M. Bramer, E. Zink, S. P. Couvillion, K. J. Bloodsworth, S. Satpathy, W. Sieh, S. M. Boca, S. Schurer, F. Chen, M. Wiznerowicz, K. A. Ketchum, E. S. Boja, C. R. Kinsinger, A. I. Robles, T. Hiltke, M. Thiagarajan, A. I. Nesvizhskii, B. Zhang, D. R. Mani, M. Ceccarelli, X. S. Chen, S. L. Cottingham, Q. K. Li, A. H. Kim, D. Fenyo, K. V. Ruggles, H. Rodriguez, M. Mesri, S. H. Payne, A. C. Resnick, P. Wang, R. D. Smith, A. Iavarone, M. G. Chheda, J. S. Barnholtz-Sloan, K. D. Rodland, T. Liu, L. Ding and Clinical Proteomic Tumor Analysis Consortium, *Cancer Cell*, 2021, **39**, 509–528.

13 U. D. Kahlert, K. Koch, A. K. Suwala, R. Hartmann, M. Cheng, D. Maciaczyk, D. Willbold, C. G. Eberhart, K. Glunde and J. Maciaczyk, *Folia Neuropathol.*, 2015, **53**, 219–225.

14 R. Zhang, P. S. Hu, Q. C. Zang, X. F. Yue, Z. Zhou, X. Y. Xu, J. Xu, S. S. Li, Y. H. Chen, B. Q. Qiang, X. Z. Peng, W. Han, R. P. Zhang and Z. Abliz, *RSC Adv.*, 2017, **7**, 24221–24232.

15 S. L. Perrin, M. S. Samuel, B. Koszyca, M. P. Brown, L. M. Ebert, M. Oksdath and G. A. Gomez, *Biochem. Soc. Trans.*, 2019, **47**, 625–638.

16 R. Liu, L. Wei and P. Zhang, *Nat. Mach. Intell.*, 2021, **3**, 68–75.

17 K. D. Rutherford, G. K. Mazandu and N. J. Mulder, *Brief. Funct. Genomics*, 2018, **17**, 34–41.

18 S. Pushpakom, F. Iorio, P. A. Eyers, K. J. Escott, S. Hopper, A. Wells, A. Doig, T. Guilliams, J. Latimer, C. McNamee, A. Norris, P. Sanseau, D. Cavalla and M. Pirmohamed, *Nat. Rev. Drug Discovery*, 2019, **18**, 41–58.

19 C. S. Greene and B. F. Voight, *Hum. Mol. Genet.*, 2016, **25**, R94–R98.

20 C. Tomi-Andrino, A. Pandele, K. Winzer, J. King, R. Rahman and D. H. Kim, *Sci. Rep.*, 2022, **12**, 11189.

21 F. B. Furnari, T. F. Cloughesy, W. K. Cavenee and P. S. Mischel, *Nat. Rev. Cancer*, 2015, **15**, 302–310.

22 A. B. Behrooz, Z. Talaie, F. Jusheghani, M. J. Los, T. Klonisch and S. Ghavami, *Int. J. Mol. Sci.*, 2022, **23**, 1353.

23 M. Hutt-Cabezas, M. A. Karajannis, D. Zagzag, S. Shah, I. Horkayne-Szakaly, E. J. Rushing, J. D. Cameron, D. Jain,

C. G. Eberhart, E. H. Raabe and F. J. Rodriguez, *Neuro Oncol.*, 2013, **15**, 1604–1614.
24 N. E. Uko, O. F. Guner, D. F. Matesic and J. P. Bowen, *Curr. Top. Med. Chem.*, 2020, **20**, 883–900.
25 S. P. Blagden, A. L. Hamilton, L. Mileshkin, S. Wong, A. Michael, M. Hall, J. C. Goh, A. S. Lisyanskaya, M. DeSilvio, E. Frangou, E. A. Stronach, P. Gopalakrishna, T. M. Meniawy and H. Gabra, *Clin. Cancer Res.*, 2019, **25**, 1472–1478.
26 C. I. Chen, H. Paul, L. W. Le, E. N. Wei, S. Snitzler, T. Wang, O. Levina, S. Kakar, A. Lau, M. Queau, J. B. Johnston, D. A. Smith and S. Trudel, *Leuk. Lymphoma*, 2019, **60**, 92–100.
27 J. Wang, X. Xu, T. Wang, Q. Guo, X. Dai, H. Guo, W. Zhang, S. Cheng, X. Chen and L. Ding, *Eur. J. Pharmacol.*, 2021, **896**, 173879.
28 B. Min, Y. Wang, F. Liang, C. X. Wang, F. Wang and Z. Yang, *Dis. Markers*, 2022, **2022**, 1832241.
29 Y. Zu, W. Wu, X. Zhao, Y. Li, W. Wang, C. Zhong, Y. Zhang and X. Zhao, *Int. J. Pharm.*, 2014, **471**, 366–376.
30 Z. Hu, L. Xuan, T. Wu, N. Jiang, X. Liu, J. Chang, T. Wang, N. Han and X. Tian, *Int. Immunopharmacol.*, 2023, **114**, 109616.
31 R. Yang, X. Yang and F. Zhang, *Curr. Neuropharmacol.*, 2023, **21**, 2097.
32 W. Q. Yao, H. Y. Gong, H. Mei, L. Shi, J. M. Yu and Y. Hu, *J. Oncol.*, 2021, **2021**, 5560915.
33 C. R. Justus, M. A. Marie, E. J. Sanderlin and L. V. Yang, *Methods Mol. Biol.*, 2023, **2644**, 349–359.
34 D. S. Wishart, A. Guo, E. Oler, F. Wang, A. Anjum, H. Peters, R. Dizon, Z. Sayeeda, S. Tian, B. L. Lee, M. Berjanskii, R. Mah, M. Yamamoto, J. Jovel, C. Torres-Calzada, M. Hiebert-Giesbrecht, V. W. Lui, D. Varshavi, D. Varshavi, D. Allen, D. Arndt, N. Khetarpal, A. Sivakumaran, K. Harford, S. Sanford, K. Yee, X. Cao, Z. Budinski, J. Liigand, L. Zhang, J. Zheng, R. Mandal, N. Karu, M. Dambrova, H. B. Schioth, R. Greiner and V. Gautam, *Nucleic Acids Res.*, 2022, **50**, D622–D631.
35 L. W. Sumner, A. Amberg, D. Barrett, M. H. Beale, R. Beger, C. A. Daykin, T. W. Fan, O. Fiehn, R. Goodacre, J. L. Griffin, T. Hankemeier, N. Hardy, J. Harnly, R. Higashi, J. Kopka, A. N. Lane, J. C. Lindon, P. Marriott, A. W. Nicholls, M. D. Reily, J. J. Thaden and M. R. Viant, *Metabolomics*, 2007, **3**, 211–221.
36 L. W. Sumner, Z. Lei, B. J. Nikolau, K. Saito, U. Roessner and R. Trengove, *Metabolomics*, 2014, **10**, 1047–1049.
37 Z. Pang, G. Zhou, J. Ewald, L. Chang, O. Hacariz, N. Basu and J. Xia, *Nat. Protoc.*, 2022, **17**, 1735–1761.
38 M. Xu, D. J. McCanna and J. G. Sivak, *J. Pharmacol. Toxicol. Methods*, 2015, **71**, 1–7.
39 B. Luzak, P. Siarkiewicz and M. Boncler, *Toxicol. in Vitro*, 2022, **83**, 105407.
40 A. M. Evans, C. O'Donovan, M. Playdon, C. Beecher, R. D. Beger, J. A. Bowden, D. Broadhurst, C. B. Clish, S. Dasari, W. B. Dunn, J. L. Griffin, T. Hartung, P. C. Hsu, T. Huan, J. Jans, C. M. Jones, M. Kachman, A. Kleensang, M. R. Lewis, M. E. Monge, J. D. Mosley, E. Taylor, F. Tayyari, G. Theodoridis, F. Torta, B. K. Ubhi, D. Vuckovic and Q. C. C. Metabolomics Quality Assurance, *Metabolomics*, 2020, **16**, 113.
41 R. Shaffer, *J. Chemom.*, 2002, **16**, 261–262.
42 C. Wieder, C. Frainay, N. Poupin, P. Rodriguez-Mier, F. Vinson, J. Cooke, R. P. Lai, J. G. Bundy, F. Jourdan and T. Ebbels, *PLoS Comput. Biol.*, 2021, **17**, e1009105.
43 M. A. Garcia-Campos, J. Espinal-Enriquez and E. Hernandez-Lemus, *Front. Physiol.*, 2015, **6**, 383.
44 Y. Xu, B. Dong, J. Wang, J. Zhang, W. Xue and Y. Huang, *OncoImmunology*, 2018, **7**, e1502130.
45 S. Riedl, B. Rinner, M. Asslaber, H. Schaider, S. Walzer, A. Novak, K. Lohner and D. Zweytick, *Biochim. Biophys. Acta*, 2011, **1808**, 2638–2645.
46 N. D. Ridgway, *Crit. Rev. Biochem. Mol. Biol.*, 2013, **48**, 20–38.
47 H. Zhou, J. H. Stafford, R. R. Hallac, L. Zhang, G. Huang, R. P. Mason, J. Gao, P. E. Thorpe and D. Zhao, *J. Biomed. Nanotechnol.*, 2014, **10**, 846–855.
48 S. Furse, N. J. Brooks, A. M. Seddon, R. Woscholski, R. H. Templer, E. W. Tate, P. R. Gaffney and O. Ces, *Soft Matter*, 2012, **8**, 3090–3093.
49 D. Rajamanoharan, H. V. McCue, R. D. Burgoyne and L. P. Haynes, *Mol. Biol. Cell*, 2015, **26**, 1428–1439.
50 S. Firdous, R. Abid, Z. Nawaz, F. Bukhari, A. Anwer, L. L. Cheng and S. Sadaf, *Metabolites*, 2021, **11**, 507.
51 S. Venneti and C. B. Thompson, *Annu. Rev. Pathol.*, 2017, **12**, 515–545.
52 R. Gorgoglione, V. Impedovo, C. L. Riley, D. Fratantonio, S. Tiziani, L. Palmieri, V. Dolce and G. Fiermonte, *Cancers*, 2022, **14**, 245.
53 K. Palanichamy, K. Thirumoorthy, S. Kanji, N. Gordon, R. Singh, J. R. Jacob, N. Sebastian, K. T. Litzenberg, D. Patel, E. Bassett, B. Ramasubramanian, T. Lautenschlaeger, S. M. Fischer, A. Ray-Chaudhury and A. Chakravarti, *Clin. Cancer Res.*, 2016, **22**, 3513–3523.
54 C. C. S. Chini, J. D. Zeidler, S. Kashyap, G. Warner and E. N. Chini, *Cell Metab.*, 2021, **33**, 1076–1087.
55 R. S. Fletcher and G. G. Lavery, *J. Mol. Endocrinol.*, 2018, **61**, R107–R121.
56 P. Gao, C. Yang, C. L. Nesvick, M. J. Feldman, S. Sizdahkhani, H. Liu, H. Chu, F. Yang, L. Tang, J. Tian, S. Zhao, G. Li, J. D. Heiss, Y. Liu, Z. Zhuang and G. Xu, *Oncotarget*, 2016, **7**, 15200–15214.
57 D. Shen, L. Tian, F. Yang, J. Li, X. Li, Y. Yao, E. W. Lam, P. Gao, B. Jin and R. Wang, *Cell Death Discovery*, 2021, **7**, 21.
58 C. R. Rocha, C. C. Garcia, D. B. Vieira, A. Quinet, L. C. de Andrade-Lima, V. Munford, J. E. Belizario and C. F. Menck, *Cell Death Dis.*, 2015, **6**, e1727.
59 R. Tjiong, P. Stavrinou, G. Rohn, B. Krischek, A. Koch, R. Goldbrunner and M. Timmer, *Anticancer Res.*, 2019, **39**, 1795–1805.
60 Z. Zhu, S. Du, Y. Du, J. Ren, G. Ying and Z. Yan, *J. Neurochem.*, 2018, **144**, 93–104.

61 A. Spencer, S. S. Yoon, S. J. Harrison, S. R. Morris, D. A. Smith, R. A. Brigandi, J. Gauvin, R. Kumar, J. B. Opalinska and C. Chen, *Blood*, 2014, **124**, 2190–2195.
62 S. V. Orlova, V. V. Tatarinov, E. A. Nikitina, A. V. Sheremeta, V. A. Ivlev, V. G. Vasil'ev, K. V. Paliy and S. V. Goryainov, *Pharm. Chem. J.*, 2022, **55**, 1133–1137.
63 N. Efsa Panel on Dietetic Products, Allergies, D. Turck, J. L. Bresson, B. Burlingame, T. Dean, S. Fairweather-Tait, M. Heinonen, K. I. Hirsch-Ernst, I. Mangelsdorf, H. J. McArdle, A. Naska, M. Neuhauser-Berthold, G. Nowicka, K. Pentieva, Y. Sanz, A. Siani, A. Sjodin, M. Stern, D. Tome, M. Vinceti, P. Willatts, K. H. Engel, R. Marchelli, A. Poting, M. Poulsen, J. Schlatter, W. Gelbmann and H. Van Loveren, *EFSA J.*, 2017, **15**, e04682.
64 X. Wang, H. Xia, F. Xing, G. Deng, Q. Shen and S. Zeng, *J. Chromatogr. B:Anal. Technol. Biomed. Life Sci.*, 2009, **877**, 1778–1786.
65 A. Herrero-Navarro, L. Puche-Aroca, V. Moreno-Juan, A. Sempere-Ferrandez, A. Espinosa, R. Susin, L. Torres-Masjoan, E. Leyva-Diaz, M. Karow, M. Figueres-Onate, L. Lopez-Mascaraque, J. P. Lopez-Atalaya, B. Berninger and G. Lopez-Bendito, *Sci. Adv.*, 2021, **7**, eabe8978.
66 J. Wood, S. J. Smith, M. Castellanos-Uribe, A. Lourdusamy, S. T. May, D. A. Barrett, R. G. Grundy, D. H. Kim and R. Rahman, *Heliyon*, 2025, **11**, e41309.